Thesis for the Degree of Master of Engineering

Dependence of upconversion luminescence on sensitizer Yb^{3+} concentration in $NaYF_4$: Yb^{3+} / Tm^{3+}

by

Hang Thi Dang

Interdisciplinary Program of

Biomedical, Mechanical & Electrical Engineering

The Graduate School

Pukyong National University

January, 2017

Dependence of upconversion luminescence on sensitizer Yb^{3+} concentration in $NaYF_4$: Yb^{3+} / Tm^{3+}

$NaYF_4$: Yb^{3+}/ Tm^{3+} 결정에서 상방전환 형광의 Yb^{3+} 농도의존성 연구

Advisor: Prof. Hyo Jin Seo

by

Hang Thi Dang

A thesis submitted in partial fulfillment of the requirements

for the degree of Master of Engineering

in Interdisciplinary Program of Biomedical, Mechanical &

Electrical Engineering, The Graduate School, Pukyong National University

January, 2017

Dependence of upconversion luminescence on sensitizer Yb^{3+} concentration in $NaYF_4$: Yb^{3+} / Tm^{3+}

A dissertation

by

Hang Thi Dang

Approved by:

_____

(Chairman: Professor Cheol Woo Park)

_____

(Member: Ph.D. Kyoung Hyuk Jang)

_____

(Member: Professor Hyo Jin Seo)

January, 2017

Contents

Dependence of upconversion luminescence on sensitizer Yb^{3+} concentration in $NaYF_4$: Yb^{3+} / Tm^{3+}

Hang Thi Dang
Interdisciplinary Program of Biomedical, Mechanical & Electrical Engineering
Pukyong National University

Abstract:

The compounds $NaYF_4$: Yb^{3+}/ Tm^{3+} with various sensitizer Yb^{3+} concentration from 0 to 100 % were synthesized by a hydrothermal method. The structure and phase purity were identified by an XRD measurement. The SEM images exhibit the expansion of hexagonal plates with increase in Yb^{3+} concentration. The effect of high excitation power and sensitizer concentration on luminescence properties in $NaYF_4$: Yb^{3+}/ Tm^{3+} compounds are investigated by spectroscopic measurements and theoretical analysis.

The $NaYF_4$: Yb^{3+}/ Tm^{3+} samples with Yb^{3+} concentration of 5, 15, 20 and 50 % were chosen for the experiments. Under the 976 nm excitation,

the excitation power density was ranged from 710 to 18900 W/cm^2. The excitation power density of 4700 W/cm^2 gives rise to almost luminescence intensities of emission bands reaching maximum values. The upconversion emission considerably quenches at higher excitation power densities than 4700 W/cm^2. At a given excitation power density, the upconversion emission exhibits unusual behavior when the concentration of Yb^{3+} ions is much high in the compounds.

1. Introduction

Luminescence upconversion (UC) is a sequential absorption of two or more photons leading to the emission of light at higher energy than the excitation energy (anti-Stock) [1- 3]. Host materials usually play a vital role in effectiveness of the UC process [2]. There are a variety of upconversion host materials among which the β-$NaYF_4$ compound has been known as the most efficient host because of low phonon energy and the high quantum efficiency [1- 2]. Lanthanide ions (Yb^{3+}, Tm^{3+}, Er^{3+}…) doped in a material possess high photostability, sharp emission bandwidths, large anti-Stock shifts [2, 4], and has potential applications in a variety of fields such as biomedical imaging, upconversion lasers and DNA detection [5- 7]. Thus, Yb^{3+}/Er^{3+} or Tm^{3+} doped in β-$NaYF_4$ has been studied in many literatures. The UC luminescence properties together with the particle sizes, crystal structures and morphologies have been reported in β-$NaYF_4$: Yb^{3+}/Er^{3+} or Tm^{3+} [1, 4, 7- 10]. The UC luminescence depends strongly on excitation power and sensitizer concentration. It is known that the UC luminescence exhibits unusual behavior in the high excitation power and high sensitizer concentration. However, there has been no report in detail on the influence of high excitation power and high sensitizer Yb^{3+} concentration on the UC luminescence.

The "Saturation" phenomenon of luminescence intensity caused by high excitation power was offered and explained in several reports. Pollnau et al suggested a simple possible model in which the intensity of an UC luminescence excited by the sequential absorption of n photons has an unusual dependence on absorbed pump power P at high excitation power density [11]. They reported the theoretical results with experimental in

$Cs_3Lu_2Cl_9$: Er^{3+}, Ba_2YCl_9: Er^{3+}, $LiYF_4$: Nd^{3+} and Cs_2ZnCl_6: Re^{4+} [11]. The decrease of slope values in Gd_2O_3: Yb^{3+}/ Er^{3+} nanowires as a result of high Yb^{3+} concentration doped and high excitation power was also reported by Yanqiang, et al in 2005 [12]. However, not many papers have been studied and estimated the saturation phenomenon of luminescence intensities in β-$NaYF_4$. In 2005, Suyer et al provided an example for the substance of the model of the excitation power dependence by using β-$NaYF_4$: 18% Yb^{3+}, 2% Er^{3+} [13], the decrease of slope values to 1 of: $^4S_{3/2} \rightarrow {}^4I_{13/2}$, $^4F_{9/2} \rightarrow {}^4I_{15/2}$, $^4S_{3/2} \rightarrow {}^4I_{15/2}$ and $^2H_{9/2} \rightarrow {}^4I_{15/2}$ transitions at high excitation power density. The dependence of upconversion luminescence on excitation power in α-$NaYF_4$: Yb^{3+}, Er^{3+} was also reported by Li et al in 2011 [14] in which the local thermal at high excitation power density considered as the main factor causing the decrease of luminescence intensities.

In this work, the dependence of luminescence intensity on the excitation power of β-$NaYF_4$: Yb^{3+}/Tm^{3+} is reported, providing another evidence for the theory of pump power affecting on luminescence properties but also helping to understand the mechanic of the "saturation" phenomenon with Tm^{3+} ions doped. On the other hand, the influence of Yb^{3+} concentration (range from 0 to 50%) on luminescence decays is investigated and discussed in detail.

2. Theoretical background

2.1 A brief introduction to luminescence

Photoluminescence (PL) is light emission from any form of matter after the absorption of photons (Electromagnetic radiation). Phosphors are luminescent materials that emit light when excited by radiation. They have many practical applications in our life and usually appear in applications such as X-ray fluorescent screens, fluorescent lamps and especial in biomedical images. The Figure 2.1 describes two ways can be used to excite an activator to obtain the emission. When the light excites directly activator, both emission and heat can be obtained. In the case of indirect excitation, the energy from excitation light can be transferred to activator from either host lattice or sensitizer [15]. The method shown in Figure 2.1b is usually applied to improve the efficiency of energy transfer from excitation source to the activator.

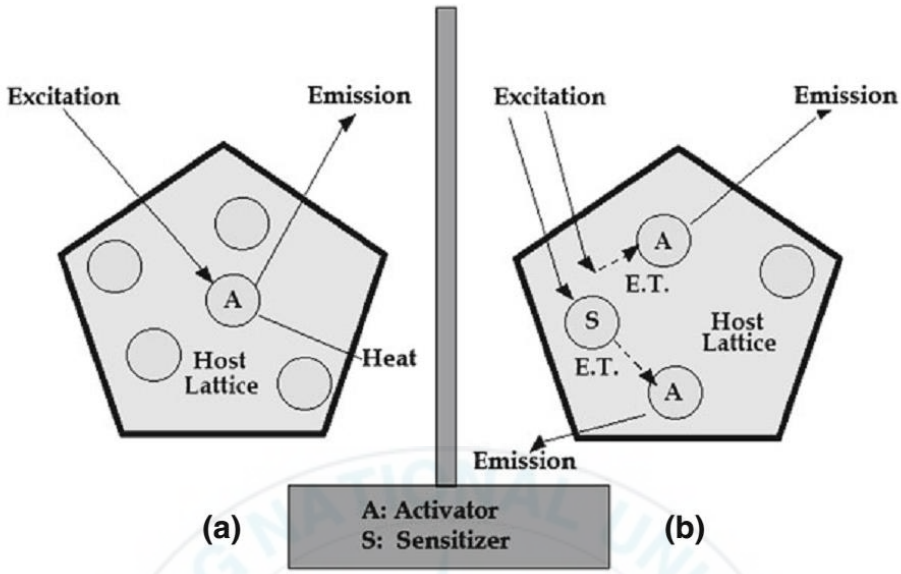

Figure 2.1 a) Schematic diagram of a direct excitation to the activator and b) the energy transferred from the sensitizer or host to the activator.

Activator

The lanthanide ions are filled with uncompleted the 4f shell and shielded by completed subshells $5s^2$ and $5p^6$. In the periodic table classic, they begin with the La and end with the Lu [15-16]. There are some lanthanide ions that have been popularly applied in applications of upconversion luminescence such as: Er^{3+}, Tm^{3+}, and Ho^{3+} [15- 17].These ions are usually doped in luminescent materials and receive excitation energy from sensitizer or directly from laser source then excited to higher states and emit light by the energy relaxation [15]. One important thing needs to be considered when choosing ions for activator is: the different energies between excited states of their ions and ground state should be close enough to facilitate photon absorption and energy transfer steps

involved in upconversion processes [15]. The ions Er^{3+}, Tm^{3+}, and Ho^{3+} have ladder-structure in their energy range, thus they are excellent candidates to improve the photoluminescence efficiency [15, 18].

The Er^{3+} ion owns a high upconversion efficiency because of the similar energy gaps between the energy levels. For instance, the energy difference in Er^{3+} between the $^4I_{11/2}$ and $^4I_{15/2}$ levels is similar to that between the $^4F_{7/2}$ and $^4I_{11/2}$ levels. Thus, the energy levels of $^4I_{15/2}$, $^4I_{11/2}$, and $^4F_{7/2}$ can be used to generate upconversion emission using 980 nm excitation [15]. Additionally, the energy dissimilar between $^4F_{9/2}$ and $^4I_{13/2}$ levels is in the same region, and thus, there are at least three different transitions in Er^{3+} ions induced by 976 nm excitation, thence causing the green and red emission light after the two sequential photons absorbed [15, 19].

Sensitizer

To improve efficiency of upconversion process, especially for NIR excitation source, some sensitizers which have a sufficient absorption cross section in this region can be doped in luminescent materials [20]. The sensitizer is a transferring energy bridge from excitation laser to activators. Yb^{3+} ion is the most popular sensitizer used in phosphors compound with doping Er^{3+} and Tm^{3+} because of simple energy level scheme with only one excited 4f level of $^2F_{5/2}$ (Fig 1.4d) which matches well with the energy transitions between the $^4I_{11/2}$ and $^4I_{15/2}$ and the $^4F_{7/2}$ and $^4I_{1/2}$ states of Er^{3+} thus improving the energy transfer efficiency between two ions [15, 21]. Similarly principle can see in Tm^{3+} and Ho^{3+}.

Host Materials

The excitation source always excites the host lattice thus the energy absorbed by the host lattice is small, the energy transferred to activators is stronger. On other hand, the host lattice also can transfer directly much energy to activators if the energy mismatch between them is small. Therefore, the host materials with low lattice phonon energy and small lattice mismatch to the dopant ion are ideal hosts for the upconversion process [15, 21].

Host lattices are constructed by Na^{+}, Ca^{2+}, Sr^{2+}, and Ba^{2+} with radius of ions approximating to those of the lanthanide dopant ions avoid the formation of crystal defects and lattice stress, therefore Na^{2+} and Ca^{2+} fluoride are admirable host materials for upconversion phosphors[15, 21]. It is known that the optical properties of upconversion materials can be considerably influenced by the crystal structure of the host materials and hexagonal $NaYF_4$ (β-$NaYF_4$) is agreed as the most efficient host material for green and blue upconversion phosphors among the fluoride hosts [1-2][4-6].

2.2 Upconversion process

The luminescence upconversion (UC) in rare-earth-doped materials is a process leading to the emission of light at higher energy than the excitation energy [1, 7]. Recently, the upconversion has been examined in a variety of host materials for potential applications in bio-optical devices.

There are several important mechanisms relating to this process such as excited state absorption (ESA), energy transfer upconversion (ETU), cooperative sensitization upconversion (CSU), cross-relaxation (CR), and photon avalanche (PA)[15, 18, 22], and they are shown in Figure 2.2 below:

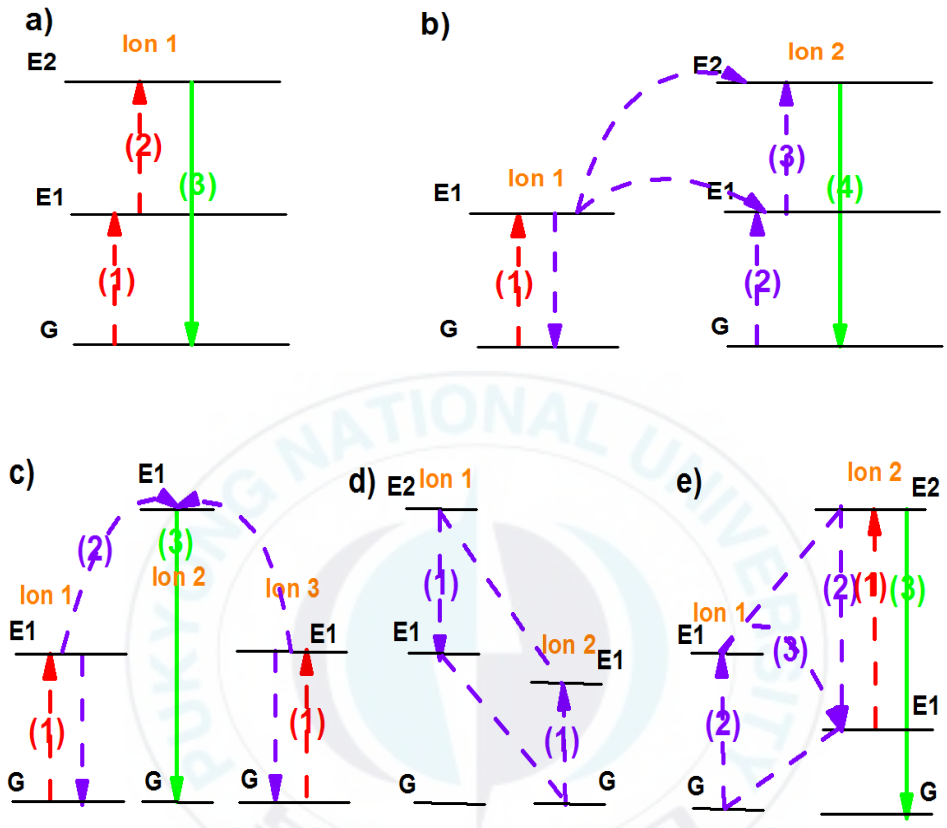

Figure 2.2 Fundamental of upconversion processes a) ESA, b) ETU, c) CSU, d) cross-relaxation (CR) and e) photo avalanche (PA).

Excited-state absorption (ESA)

A single ion at the ground state absorbed the energy from excitation source and is excited to higher energy level E1 (Figure 2.2 a), a second pump photon that promotes this photon from E1 to higher state E2. A radiative emission is obtained when the photon relaxes from the E2 state to the ground state. Some lanthanide ions for example: Er^{3+}, Ho^{3+}, Tm^{3+} and Nd^{3+} have such energy level structures which also find a good excitation

wavelength match with the output of commercially available diode lasers (976 nm or 808 nm) are usually applied to improving the efficient upconversion processes [1, 2, 23].

Energy Transfer Upconversion (ETU)

ETU process involves two neighboring ions, one photon known as sensitizer photon and the other photon known as an activator [2]. Firstly, after absorbing a pump photon, the sensitizer ion (ion 1) is excited from the ground state to its metastable level E1, then transfers its energy to the ground state (G) of ion 2, pumping this ion to an excited state. If the second ion is already in an excited state, the energy transfer will pump it to an even higher-energy excited state (E2).

While the dopant concentration has much influence on the upconversion efficiency of an ETU upconversion process because of determining the average distance between the neighboring dopant ions, the upconversion efficiency of an ESA process is independent of the dopant concentration due to its single ion characteristic [2].

Cooperative sensitization upconversion (CSU)

CSU process is shown in Figure 2.2c with taking part in of three photons. Assume that the first and third ions are sensitizers in ETU process. After absorbing energy from excitation source, these ions can be excited to the metastable state E1, respectively. Then transfer their energy to the ion number 2 (which does not need to have an intermediate excited state), pumping to excited state. The excited ion 2 can emit an upconverted photon by relaxing back to the stable state [2].

Cross-relaxation (CR)

CR process is a result of the interaction between two same or different ions in which ion 1 transfers part of its excited energy to ion 2 through a process of E2(ion 1) +G(ion 2) → E1 (ion 1) + E1(ion 2) [2, 15]. If two these ions are the same, cross-relaxation process will facilitate "concentration quenching mechanism" which significantly quenches the emission intensity.

Photon Avalanche.

Photon avalanche is an unusual upconversion process that is dependent on pump intensity value. There are a threshold value which determines either little or strong luminescence. A very weak intensity of luminescence is produced when the excitation power intensity is smaller than threshold value that is lower than the pump intensity causing a strong light emission [18, 24].

In fact, the PA process involves two processes of ESA for excitation light and an efficient CR that produces feedback. Firstly, after populating to level E1 by non-resonant weak ground state absorption, ion 2 is excited to upper visible-emitting level E2 by a resonant ESA process. Then, an efficient CR process of E2 (ion 2) + G (ion 1) → E1 (ion 2) + E1 (ion 1) between ion 1 and ion 2 occurs, resulting in both ions occupying the intermediate level E1. A strong UC emission as an avalanche process is produced by two ions populated level E2 to further initiate cross-relaxation and exponentially increased level E2 population by ESA [2]. In addition to high pump intensity, photo avalanche induced upconversion also requires long response time to excitation source.

2.3 Theory of anomalous power dependence

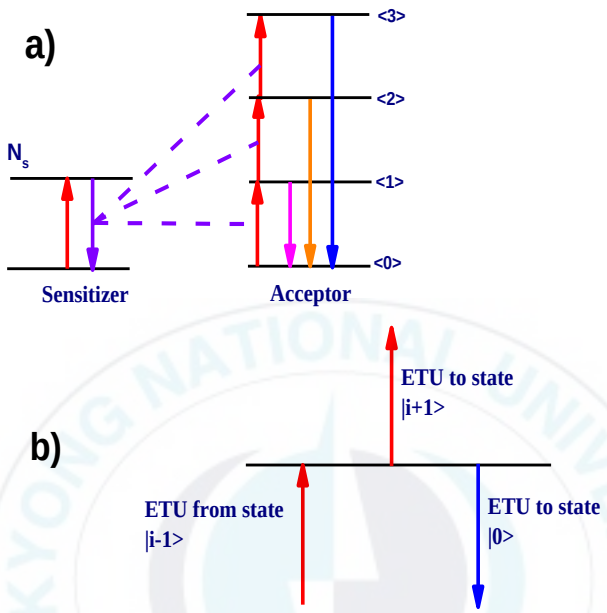

Figure 2.3 a) Schematic of energy transfer from a sensitizer to an acceptor and b) The populating and depopulating processes for a general state |i> of the acceptor ion.

The anomalous power dependence occurs at very high laser powers when the number of photons required to generate an ideal upconversion process equals 1 for all of emission bands. This phenomenon can be explained by the theory of competition between linear decays and upconversion processes for the depletion of the intermediate excited states which was theoretically described by Pollnau el at [11, 13].

Figure 2.3a describes the energy transfer from a sensitizer to an acceptor which has four energy ladders |0>, |1>, |2> and |3>. In the ideal case, the

energy at the state |1> of the acceptor ion and the excited state of sensitizer should be same or in other words, the population of state |1> of the acceptor ion scales linearly with the laser power.

$$N_1 \sim N_s$$

A simple model describing the population and depopulation of a general state |i> is shown in Figure 2.3b. Let N_i, N_s denote the steady state population density of the state |i>, and excited state population density of the sensitizer ion, respectively. Moreover, the upconversion rate constant for upconversion process from state |i> to state |i+1> on the acceptor ion will be denoted by W_i, and R_i will be the rate constant for relaxation process from state |i> to the ground state. This total emission rate constant includes both nonradiative multiphonon relaxations as well as radiative emission.

Under the assumptions described above, one can directly write down the balance equation for the steady state population density of state |i> of the acceptor ion,

$$W_{i-1}N_{i-1}N_s = (R_i + W_iN_s)N_i$$

This balance equation can be written to find the steady state population density of state |i> by:

$$N_i = (W_{i-1}N_{i-1}N_s)/(R_i + W_iN_s)$$

There are two situations with the limitation of excitation power. The first case is a low power limit, when there is not enough energy transfer to populate at high levels owing to depopulation processes being dominant or $R_i >> W_iN_s$ and the result is $N_i \sim N_s \sim P^i$. In consequence, emission bands that require |i> energy transfer upconversion steps to be excited will have exactly a slope of |i> at double logarithmic representation.

In the case of high excitation power density, population processes are more efficient than depopulation because of strong energy transfer from Yb^{3+} ions to Tm^{3+} ions. Therefore, population process becomes easier or in other words $W_iN_iN_s >> R_iN_i$ and the results is $N_i \sim N_s \sim P^1$ leading to emission band of the acceptor ions will have a slope of 1.

3. Experiment section

3.1 Experimental chemical reagents and synthesis equipment

Table 3.1 List of the chemical reagents that are used in sample synthesis

No	Reagents	Purity (%)	F.W(g)	Manufacturer
1	Y_2O_3	99.9	225.82	Sigma-Aldrich. Chemie. GmbH
2	Yb_2O_3	99.99	394.08	Wako. Pure Chemical Industries. Ltd
3	Tm_2O_3	99.95	385.86	Wako. Pure Chemical Industries. Ltd
4	HNO_3	60	63.01	Daejung chemicals & metals company
5	NaF	99	41.99	Fuluka Chemika
6	NH_3OH		34.01	Daejung chemicals & metals company
7	CH_3CH_2OH	99.5	46.07	Daejung chemicals & metals company
8	$Na_3C_6H_5O_7$	99.5	258.07	Daejung chemicals & metals company

Some equipment are required for the synthesis process such as: Teflon vessels, oven, stainless steel autoclaves and magnetic stirrer.

3.2 Sample preparation

All the chemicals of Y_2O_3 (99.99%), Yb_2O_3 (99.99%), Tm_2O_3 (99.99%), $Na_3C_6H_5O_7$ (99.5%), NaF (99%), HNO_3, NH_3.OH were obtained from chemical reagent factories and used as the starting materials without any further purification. The $NaY_{1-x}Yb_xF_{4:}Tm^{3+}$ crystal forms a solid solution up to Yb^{3+} ions at a concentration of 100% were prepared. Three lanthanide oxides R_2O_3 (R=Y, Yb, Tm) were firstly dissolved in acid nitric 60% at an elevated temperature. Next, the residual acid was removed by adding deionized water and heating up, repeated in four times. The final obtained solution of this step was $R(NO_3)_3$ 0.2M solution. These solutions were then added into 32 ml aqueous solution (16 mmol sodium citrate $Na_3C_6H_5$) and stirred strongly for 30 minutes to form a chelated RE-citrate complex which was then added 40 ml aqueous solution containing 24 mmol NaF. After stirring for 60 minutes (the pH value for this mixture were always kept at 9), the final complex was introduced into a Teflon-lined stainless steel autoclave and heated at 230^oC for 20 hours. The autoclave was cooled at room temperature. After that, the precipitate was collected and washed in 5 times with deionized water and ethanol, and finally dried at 100^oC for 2.5 hours. To study the effect of Yb^{3+} ions content on the luminescence properties, the phosphor with different Yb^{3+} concentration were obtained

through changing the added difference amount of Yb_2O_3, Y_2O_3 under similar condition.

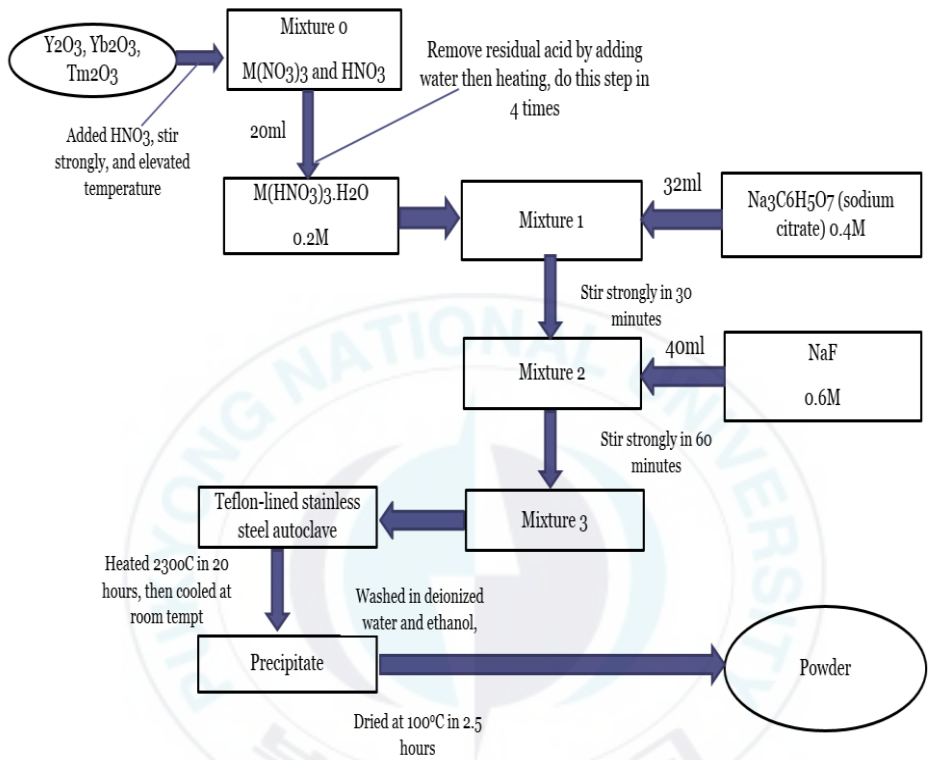

Figure 3.1 The flow chart of preparation process of $NaYF_4$: Yb^{3+}/Tm^{3+}

Table 3.2 Detail of a mount of reagents contributed in synthesis process

Sample (%Yb^{3+})	Y_2O_3 (mmol)	Weight (g)	Yb_2O_3 (mmol)	Weight (g)	Tm_2O_3 (mmol)	Weight (g)
0	2	0.452	0	0	0.02	0.004
5	1.9	0.429	0.1	0.0394	0.02	0.004
15	1.7	0.384	0.3	0.118	0.02	0.004
30	1.4	0.316	0.6	0.237	0.02	0.004
50	1	0.226	1	0.394	0.02	0.004
70	0.6	0.136	1.4	0.552	0.02	0.004
90	0.1	0.226	1.9	0.749	0.02	0.004
100	0	0	2	0.789	0.02	0.004

3.3 Measurement

The structure and phase of samples were determined by XRD while the morphology results were obtained by SEM experiments. XRD measurement was carried out on a Rigaku D/Max diffractometer operating at 40KV, 30mA with Bragg-Brentano geometry using Cu-Kα1 radiation (λ=0.15406 nm). The 2θ angle ranging from 10 to 70° were collected in a scanning mode with a step size of 0.02° and a rate of 4.0°min^{-1}. The

morphologies of the samples were observed by means of a field emission scanning electron microscopy (FE-SEM, Japan, Hitachi, S-4800).

Optical measurement

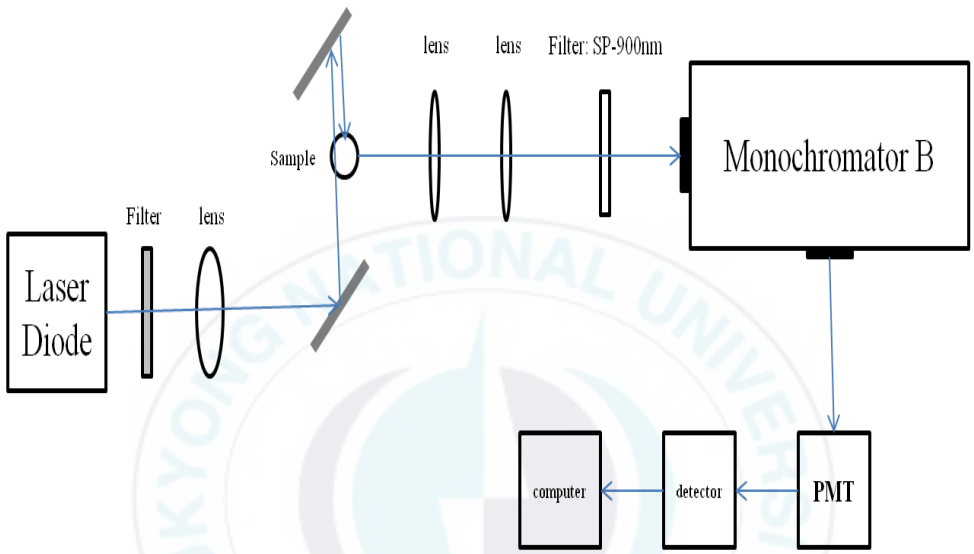

Figure 3.2 The schematic map of upconversion measurement

A diode laser tuned to 976 nm was used for upconversion spectroscopic experiment as the pump source inclined 45° to irradiate the center of the samples.

4. Results and discussion

4.1 XRD and SEM results

XRD results

The structure and phase purity of samples were identified by powder XRD analysis. Figure 4.1a shows the XRD patterns of $NaYF_4$: Yb^{3+}/ Tm^{3+} for various Yb^{3+} concentrations from 0 to 100%. The synthesized materials show strongly defined and sharp reflections in the XRD patterns, confirming the good crystallinity and high purity of the product.

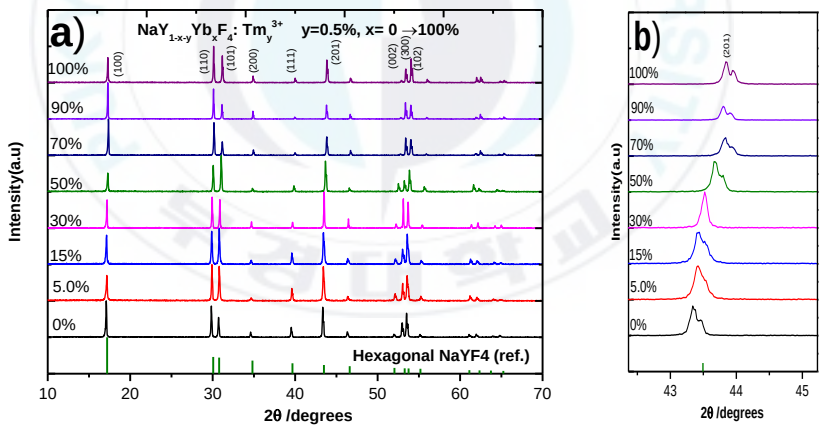

Figure 4.1 a) XRD patterns of β-$NaYF_4$ crystals doped with 0.5 %Tm^{3+} and 0, 5, 15, 30, 50, 70, 90 and 100 %Yb^{3+}, b) Red shift

Figure 4.1b shows that the peaks shift towards higher diffraction angles with increasing Yb^{3+} concentration indicating the reduction in unit cell volume (Bragg's equation) [24] by the substitution of Y^{3+} ions (r=1.159 Å) [25] by smaller Yb^{3+} ions (r=1.125 Å) [25] in the host lattice.

Morphology

Figure 4.2 presents the SEM images of hexagonal β-$NaYF_4$: Yb^{3+}/ Tm^{3+}, where Yb^{3+} concentration are 0, 30 and 90 %. As can be seen clearly, these samples exhibit a uniform hexagonal shape and increase in the size with increasing Yb^{3+} concentration (Table 4.1).

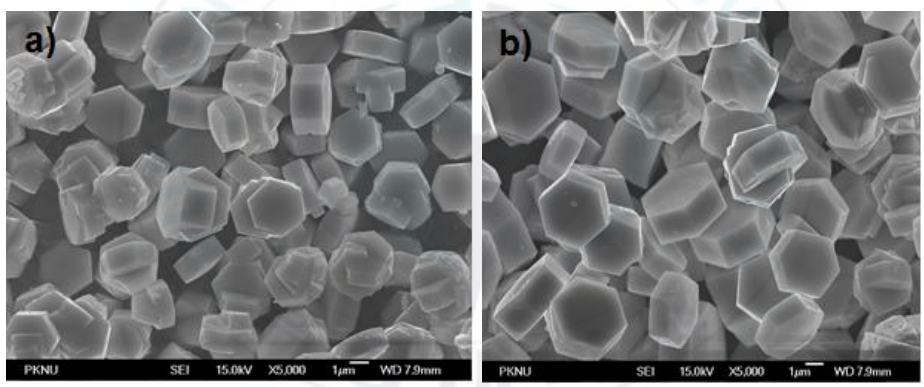

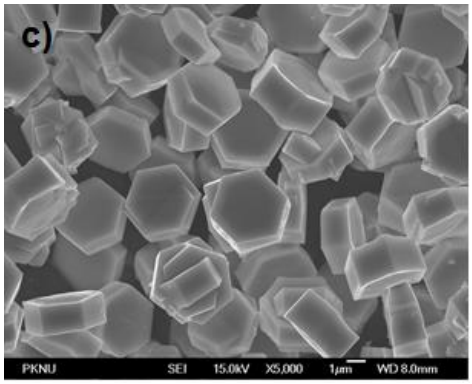

Figure 4.2 SEM results for hexagonal structure β-$NaYF_4$: Yb^{3+}/Tm^{3+} with Yb^{3+} concentration of a) 0, b) 30, c) 90 %.

Table 4.1 The increases of crystal size of β-$NaYF_4$: Yb^{3+}/Tm^{3+} when the concentration of Yb^{3+} changes

Sample	**Width(μm)**	**Thickness(μm)**
0% Yb^{3+}	2.6	1.6
30% Yb^{3+}	3.2	1.6
90% Yb^{3+}	3.4	1.8

The expansion of the plates with increase in Yb^{3+} concentration can be explained by the electron charge density of the crystal surface theory.

Liu at al (2010) [26] reported that the electron charge density of crystal surface $NaYF_4$: Yb^{3+}/Er^{3+} increases after substituting a Gd^{3+} ion with a larger ionic radii (r=1.193 Å) [25] for Y^{3+} ion with r=1.159 Å [25]. Figure 4.3 shows the crystal structure of hexagonal phase $NaYF_4$ consists of F-ions. There exists two types of cation sites selectively occupied by Na^+ and RE^{3+} ions. This results in significant electron cloud distortion of the cations

to accommodate the structural change [26- 27]. The Yb^{3+} (r=1.125 Å) [25] with a smaller radius substituted for Y^{3+}ions causes the decrease of surface electron charge density facilitating diffusion of the negative F^- ions towards $NaY_{1-x}Yb_xF_4$ crystal nuclei, which will accelerate the growth of the nanocrystals. To lower the surface energy, the $NaY_{1-x}Yb_xF_4$ hexagonal particles aggregate and self-assemble [26- 27]. Figure 4.4 shows the possible formation mechanism for the β-$NaYF_4$: Yb^{3+}/Tm^{3+} crystals with different Yb^{3+} concentrations.

The samples were synthesized under high temperature (230 ^oC) and heated in 20 hours, thus the initial form of $NaYF_4$ is the hexagonal shape. The small hexagonal particles of the $NaYF_4$: Tm^{3+} sample has a tendency to aggregate and self-assemble to become a bigger particle by co-doping of Yb^{3+} ions. When 30% Yb^{3+} doped in the crystal lattice of $NaYF_4$, as mentioned above, the surface electron density of the small particles decreases causing a stronger aggregation of these particles. Many particle units aggregate together and create new particles which are bigger than purity $NaYF_4$ particles. This phenomenon in 90%Yb^{3+} doped sample is more dominant leading to the increase in particle size.

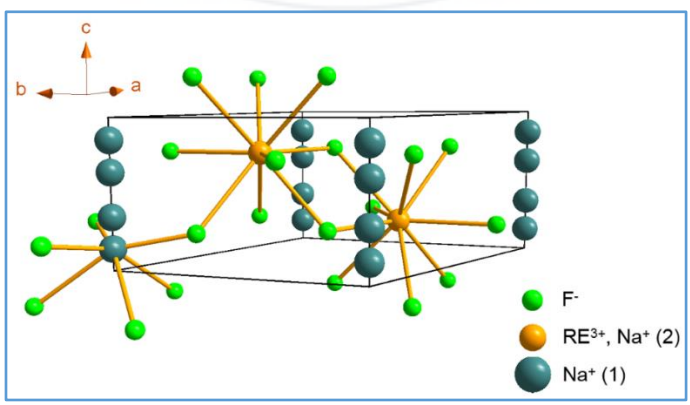

Figure 4.3 Schematic presentation of hexagonal-phase $NaYF_4$ structure

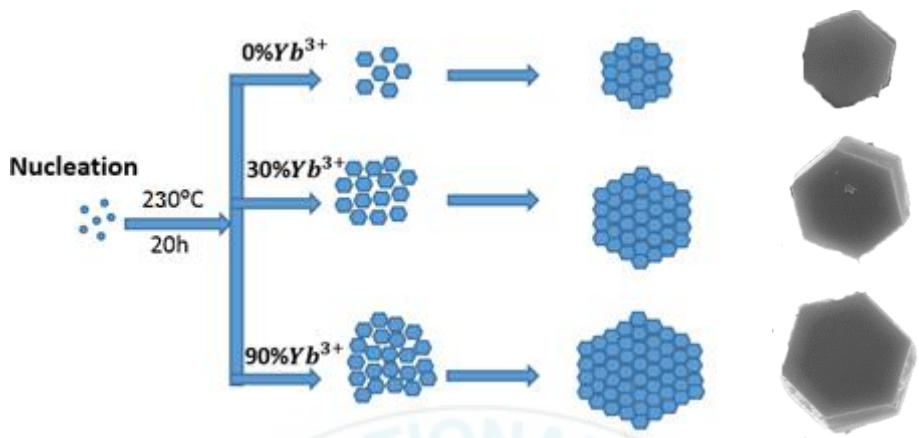

Figure 4.4 Schematic representation of formation procedure of β-$NaYF_4$: Yb^{3+}/ Tm^{3+}(0.5 %) with different Yb^{3+} concentration.

4.2 Mechanism of the upconversion luminescence

The mechanism for NIR to NIR UC photoluminescence is explained by energy diagram in Figure 4.5 [1, 4, 28].

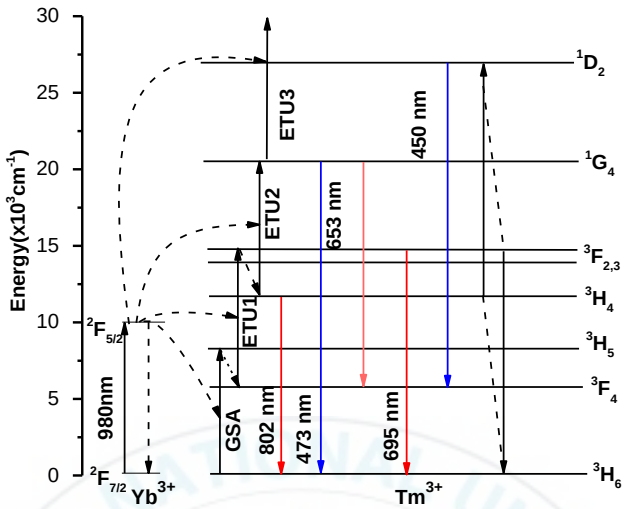

Figure 4.5 The mechanism of luminescence emissions in Yb^{3+}/Tm^{3+}

The corresponding input photons can excite only the Yb^{3+} ions because there is no such excited energy level above the ground state of Tm^{3+} ions. After 976 nm excitation, Yb^{3+} ions transfer energy to the neighboring Tm^{3+} ions. Four successive energy transfers from Yb^{3+} to Tm^{3+} populate the $^3H_5$, $^3F_2$, $^1G_4$ and $^1D_2$ levels of Tm^{3+} ion (Figure 4.5). These energy transfer processes along with some radiative relaxations are responsible for the 450 nm ($^1D_2 \rightarrow {}^3F_4$), 473 nm ($^1G_4 \rightarrow {}^3H_6$), 653 nm ($^1G_4 \rightarrow {}^3F_4$), 695 nm ($^3F_{2,3} \rightarrow {}^3H_6$) and 802 nm ($^3H_4 \rightarrow {}^3H_6$) emission bands. The first energy transfer process (GSA) excites the $^3H_6$ state to the $^3H_5$ state with the redundant energy dissipated by photons. Subsequently, the Tm^{3+} ion relaxes nonradiatively

to the lower $^3F_4$ state and further populates the $^3F_{2,3}$ state through a second energy transfer process (ETU1). The weak 695 nm emission band is associated with the radiative transition from the $^3F_{2,3}$ state to the ground state. Additionally, the strong NIR emission with a peak at 802 nm arises from the $^3H_4 \rightarrow {}^3H_6$ transition, where the $^3H_4$ state is populated by the efficient nonradiative relaxation from the $^3F_{2,3}$ state. Third energy transfer process (ETU2) excites the $^3H_4$ state to the $^1G_4$ state from which the emissions peaked at 473 and 653 nm are generated corresponding to the $^1G_4 \rightarrow {}^3H_6$ and $^1G_4 \rightarrow {}^3F_4$ transitions, respectively. Because of large energy gap between the $^1G_4$ level and the $^1D_2$ level, there are no excited photon from $^1G_4$ to $^1D_2$ state. The population at the $^1D_2$ state is contributed by fourth energy transfer from Yb^{3+} ion and nonlinear interaction process $^3F_2 + {}^3H_4 \rightarrow {}^3H_6 + {}^1D_2$ of two adjacent Tm^{3+} ions [1, 29].

4.3 The influence of Yb^{3+} concentration on upconversion luminescence

We investigate the dependence of luminescence intensity as a function of excitation power density for various Yb^{3+} concentration in $NaYF_4$: Yb^{3+}/Tm^{3+} system. A 976 nm NIR excitation in the range of power density from 700 to 18900 W/cm^2 was applied on the 5, 15, 20 and 50 % Yb^{3+} doped samples. Obtained results are shown in Figure 4.6. For all the samples, five main emission bands centered at 450 nm, 473 nm, 653 nm, 695 nm and 802 nm corresponding to $^1D_2 \rightarrow {}^3F_4$, $^1G_4 \rightarrow {}^3H_6$, $^1G_4 \rightarrow {}^3F_4$, $^3F_3 \rightarrow {}^3H_5$ and $^3H_4 \rightarrow {}^3H_6$

transitions are observed. It is interesting to note that the intensity of the $^3H_4 \rightarrow {}^3H_6$ transition and the relative intensity between the transitions $^1D_2 \rightarrow {}^3F_4$ and $^1G_4 \rightarrow {}^3H_6$ change systematically with increasing Yb^{3+} concentration depending on the excitation power density.

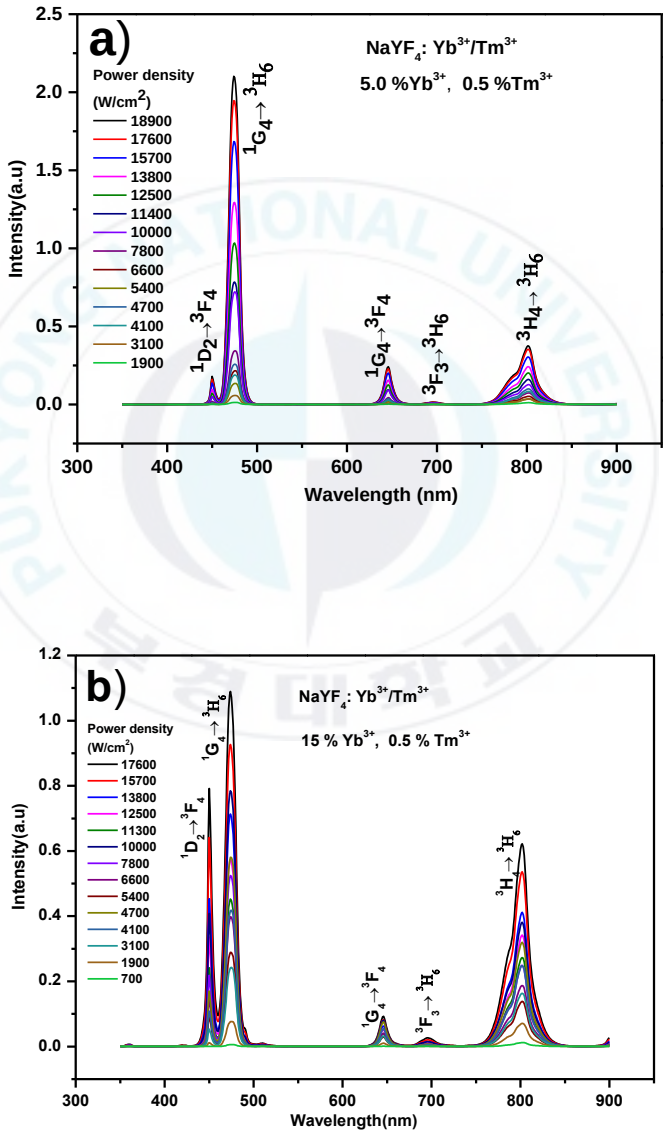

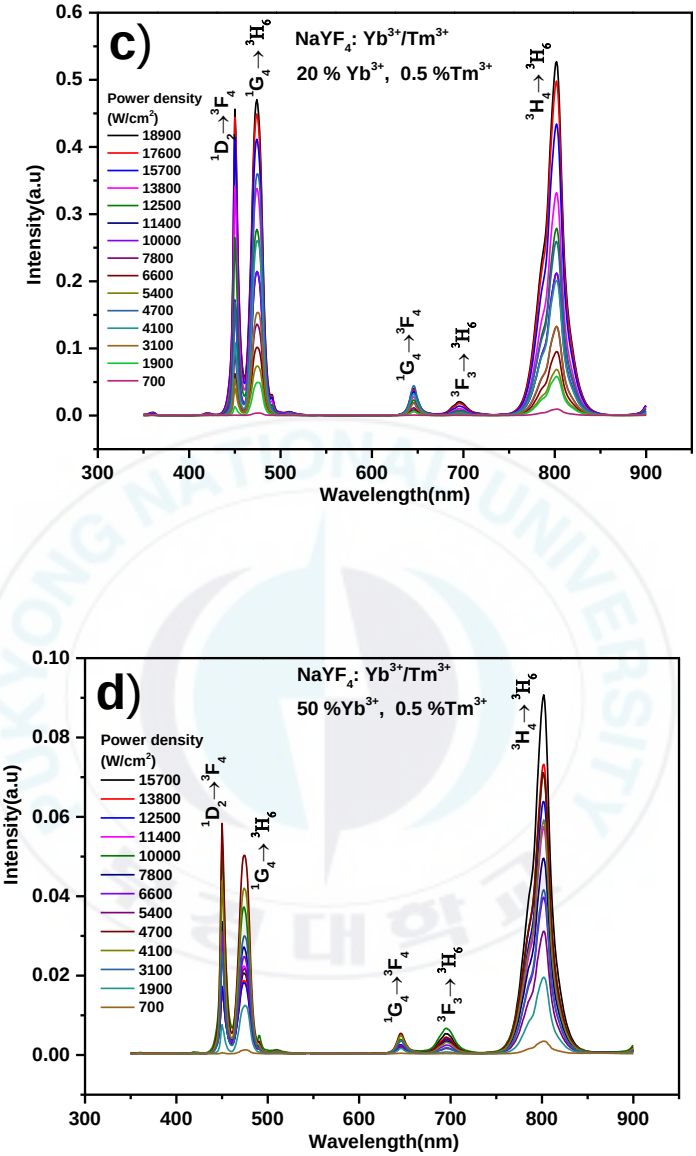

Figure 4.6 Photoluminescence spectra under 976 nm wavelength excitation in the range of excitation power density from 700 to 18900 W/cm^2 of NaYF4: Yb^{3+}/Tm^{3+} with a) 5, b) 15, c) 20, d) 50 % Yb^{3+} doped.

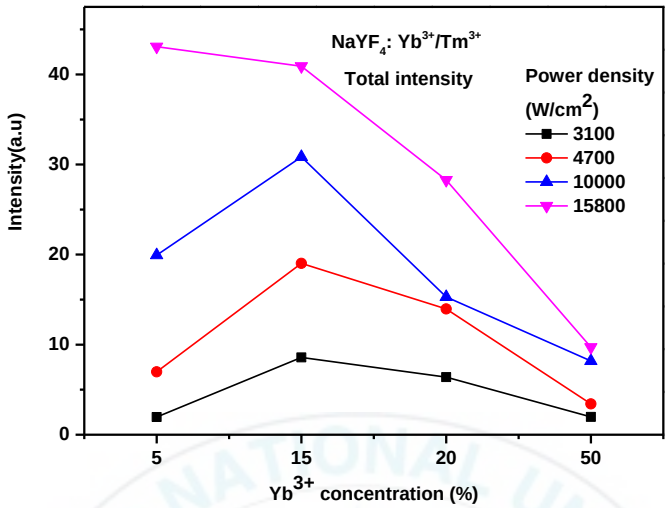

Figure 4.7 The dependence of total luminescence intensity on excitation power density and Yb^{3+} concentration doped

Figure 4.7 shows the total luminescence intensity of four samples 5, 15, 20 and 50 % at different excitation power density of 3100, 4700, 10000 and 15800 W/cm^2. Under the excitation power density of 3100, 4700 and 10000 W/cm^2, the intensities increase quickly from Yb^{3+} concentration of 5 to 15 % because of the quick enhancement of energy transfer probabilities of Yb^{3+} - Yb^{3+}, Yb^{3+} - Tm^{3+} ions, then the upconversion emission quenches considerably for the samples of 20, 50 % Yb^{3+} doped. At the highest excitation power density of 15800 W/cm^2, the intensities of luminescence decrease along with the increase of Yb^{3+} concentration. This phenomenon can be explained by the anomalous behavior of upconversion luminescence [13], which is induced by the competition between population and depopulation processes for the depletion of the intermediate excited states (detailed in Figure 4.11). At high excitation power density or high

concentration of sensitizer doped, the luminescence intensity starts quenching.

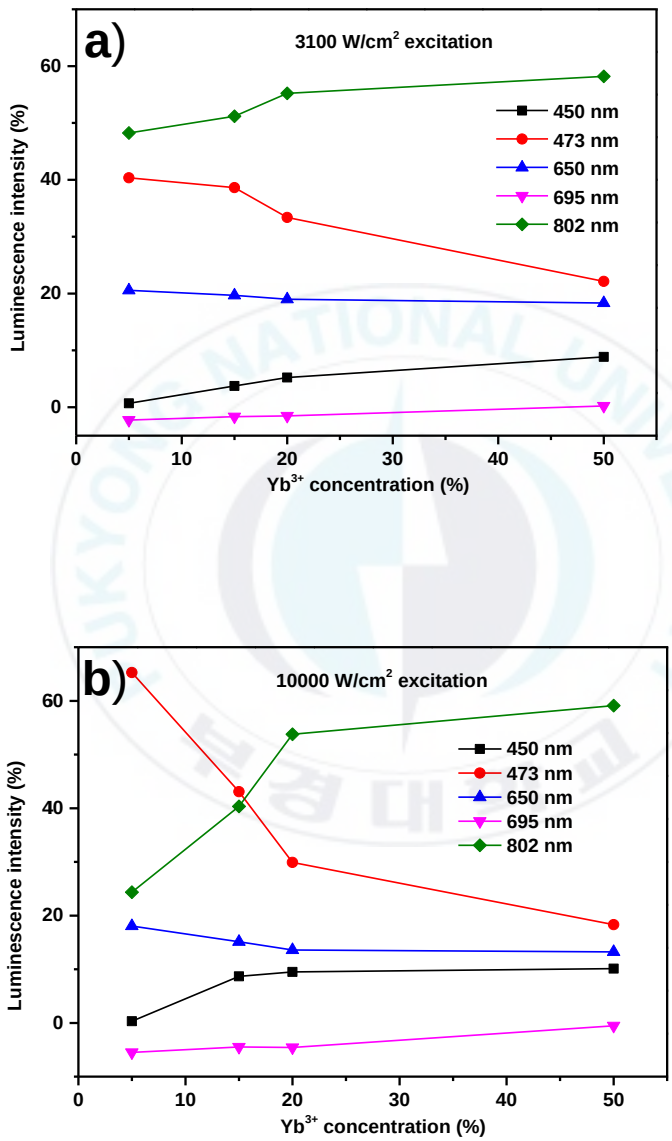

Figure 4.8 The contributed percentages in luminescence intensity of five emission bands at a) 3100 W/cm^2, b) 10000W/cm^2 excitation

Figures 4.8a and b show the changes of intensity at the emitting state of $^1D_2$, $^1G_4$, $^3F_{2,3}$ and $^3H_4$ to the total intensity as a function of sensitizer Yb^{3+}concentration for low power (3100 W/cm^2) and high power excitation densities (10000 W/cm^2). For the two excitation power densities, the upconversion intensity of the $^1D_2 \rightarrow {}^3F_4$ transition increases with increasing Yb^{3+} concentration, while the intensity of $^1G_4 \rightarrow {}^3H_6$ transition decreases. We note that the increasing rate of $^1D_2$ and the decreasing rate of $^1G_4$ is higher for the high power excitation as in Figure 4.8b.

For the excitation intensity of 3100 W/cm^2, the 5 % Yb^{3+} doped sample show that the intensity percentage of the 450 nm $^1D_2$ emission band is very weak only about 0.007 to the total upconversion intensity as shown in Fig. 4.7a. When Yb^{3+} concentration increases to 15 %, this value in total luminescence intensity is 0.038 and it becomes 0.2 and three times in 50 % Yb^{3+} doped samples. The contribution of ($^1G_4$) 473 nm emission band to total emission intensity decreases slightly 0.02, 0.05 and 0.1 with Yb^{3+} ion concentration at 15, 20 and 50 %, respectively. Similarly, the intensity proportion of ($^1G_4$) 650 nm emission band decreases inconsiderably (0.002) when the increase of Yb^{3+} concentration is from 5 to 20 %, this proportion decreases quickly approximately 0.1 at 50 % Yb^{3+} doped. The emission intensity of $^3F_3 \rightarrow {}^3H_6$ (695 nm band) transition increases along with

increasing of Yb^{3+} doped concentration. It is seen that no emission for this transition in the sample of 5 % Yb^{3+} doped, then becomes significantly at 50 % Yb^{3+} doped with 0.0025 in total luminescence intensity. In all the four measured samples, the proportion in total luminescence intensity of ($^3F_4$) 802 nm band is highest among five main emission bands. This values rise slowly about 0.01 along the increase from 5 to 50% of Yb^{3+} doped concentration.

Under 10000 W/cm^2 excitation, the decrease of 473 and 650 nm emission bands and the increase of 450, 695 and 802 nm emission bands in contributed luminescence percentages are clearly observed (Figure 4.8b). The enhancement in the 450, 695, 802 nm and the quenching in the 475, 650 nm emission bands come from the increase of energy transfer probabilities Yb^{3+} - Yb^{3+} sensitizers, Yb^{3+} - Tm^{3+} ions and cross-relaxation processes between two Tm^{3+} ions at high Yb^{3+} concentration doped. The increased Yb^{3+} ion concentration increases the sensitization by absorbing more NIR photons and enhances the Yb^{3+} to Yb^{3+} energy migration as well as the Yb^{3+} to Tm^{3+} energy probability, which leads to the increase of the population at $^1D_2$ and $^3F_3$ states causing the increase of 450 nm ($^1D_2 \rightarrow {}^3F_4$). Moreover, the cross-relaxation probability between two Tm^{3+} ions are improved considerably due to the increase of population density of energy states. The $^3F_2 + {}^3H_4 \rightarrow {}^3H_6 + {}^1D_2$ process played an important role in populating the $^1D_2$ level [1, 29] generating 450 nm emission band. This process also can be used to explain the slope value calculated for $^1D_2 \rightarrow {}^3F_4$ transition. In the case of not enough energy transfer to populate $^1D_2$ state (four photons), the emission of 450 nm band can occur by the $^3F_2 + {}^3H_4 \rightarrow$

$^3H_6$ + $^1D_2$ nonlinear interaction process (Figure 4.9) which requires three photons. The increase in percentage of intensity of 802 nm emission band is a result of cross- relaxation processes $^1D_2$ + $^3H_6$→ $^3F_3$ + $^3H_4$ and $^1D_2$ + $^3H_6$→ $^3H_4$ + $^3F_2$ (Figure 4.9) [1]. The luminescence of 695 nm ($^3F_3$→$^3H_6$) emission band increases along with the increase of excitation power density and Yb^{3+} concentration. This can be explained by the increase of the second order of the peak at 345 nm emission band [1, 30].

The increase of energy transfer probability improves the population density of higher states ($^1D_2$) while causes the decrease of the population at lower levels ($^1G_4$), which leads to the quench of transitions from this level such as: $^1G_4$ →$^3H_6$ (473 nm emission band) and $^1G_4$→$^3F_4$ (650 nm emission bands).

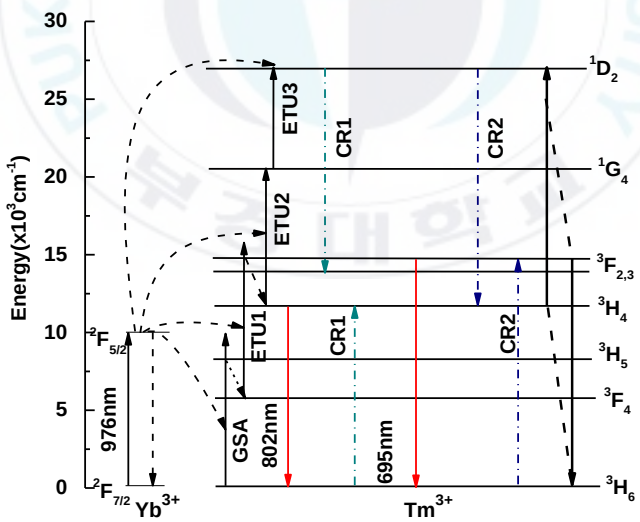

Figure 4.9 Cross-relaxation and nonlinear interaction processes in Tm^{3+} energy levels

To make clear the influence of high excitation power density and Yb^{3+} doped concentration on luminescence intensity properties, the log-log plot of the emission intensity as a function of excitation power are shown in Figure 4.10 for 450, 473, 695 and 802 nm emission bands.

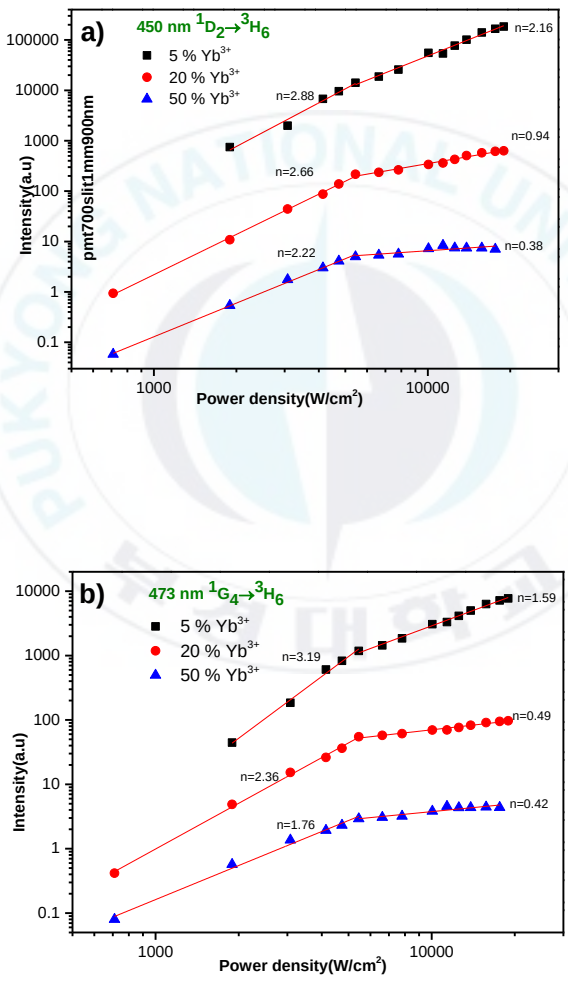

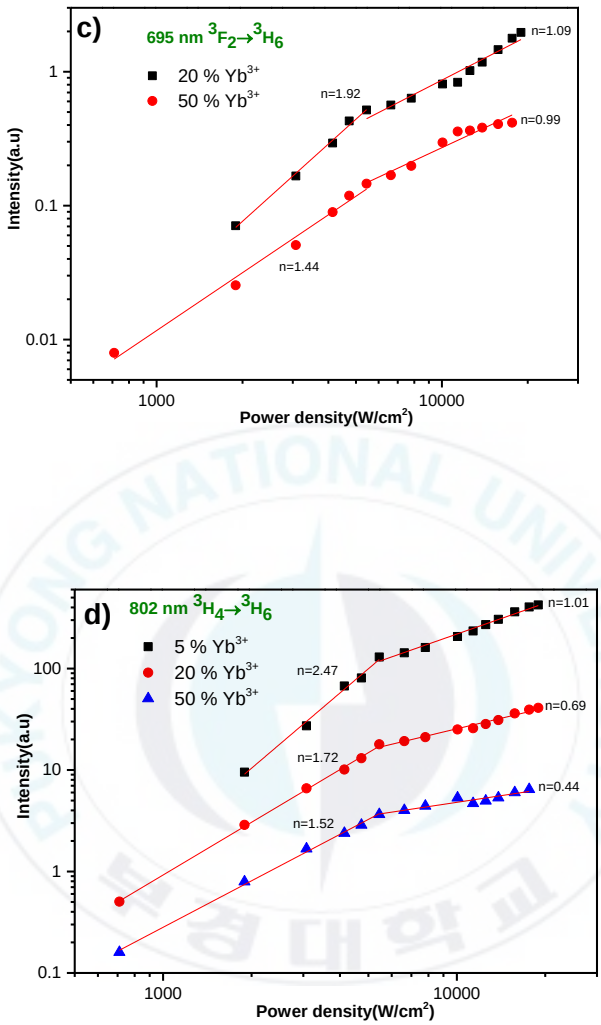

Figure 4.10 Log - log plot of the emission intensity as a function of excitation power a) $^1D_2 \rightarrow {}^3F_4$, b) $^1G_4 \rightarrow {}^3H_6$, c) $^3F_3 \rightarrow {}^3H_6$, and d) $^3H_4 \rightarrow {}^3H_6$ transitions.

Figure 4.10a describes upconversion luminescence intensity as a function of excitation power density of 450 nm emission band calculated

for different Yb^{3+} doped samples. The slope value is 2.88 at 5 % Yb^{3+} doped. It confirms that there are three photons required for upconversion processes to emit this emission band. After decreasing to 2.66 at 20 % Yb^{3+} doped, the slope value falls to 2.22 when Yb^{3+} ion concentration of 50 %. At 5 % Yb^{3+} doped, there is a slight quenching in the slope value from 2.88 to 2.16 when high excitation power densities were applied. For the 20 and 50 % samples, the slope values start decreasing strongly to 0.94 and 0.38 with increasing of excitation power density from 4700 to 18900 W/cm^2. Before the saturation point (at 4700 W/cm^2 excitation), the slope value for the transition of $^1G_4 \rightarrow {}^3H_6$ is 3.19 at 5 % Yb^{3+} doped, it means that the upconversion processes involve at least three photons to emit 473 nm emission band. The slope values reduce strongly along the increase of Yb^{3+} doped from 5 to 50 % with 3.19 to 1.76, respectively. At 4700 W/cm^2 excitation power density, the slope values of all of three samples start falling to 1.59, 0.49 and 0.42 at 5, 20, 50 % Yb^{3+} doped, respectively.

For the emission band of 695 nm at 5 % Yb^{3+}, no upconversion emission is observed. At the Yb^{3+} concentration of 20 %, the slope value of this band is 1.92 confirming two photons processes required for this emission. The value then decreases to 1.44 in 50 % Yb^{3+} sample. Similar phenomenon with 473 nm emission band, the slope value starts decreasing when excitation power densities are over 4700 W/cm^2, there are 1.09 for 20 % Yb^{3+} and 0.99 for 50 % Yb^{3+}.

The obtained slope value of 802 nm emission band is 2.47 for 5 % Yb^{3+} doped before 4700 W/cm^2 excitation power density, which confirms that at least two photons for upconversion processes should be required to emit 802 nm band. The slope values drop to 1.72 and 1.52 at 20 and 50 % Yb^{3+}

doped, respectively. After 4700 W/cm^2, the slope values of three samples 5 , 20 and 50 % Yb^{3+} doped fall to 1.01, 0.69 and 0.44, respectively.

The noticeable decrease of slope values at high excitation power density or high concentration of Yb^{3+} can be particularly explained by the simple model, which was built by M. Pollau [11, 13].

At first, N_1, N_2 and N_3 denote the steady state population density of states $^3F_4$, $^3H_4$ and $^1G_4$ (Figure 4.11); N_{Yb} denotes (also steady state) the excited state population density at $^2F_{5/2}$ of Yb^{3+} ion. Furthermore, W_1, W_2 and W_3 will denote the upconversion rate constant associated with upconversion of $^3H_6$ - $^3F_4$, $^3F_4$ - $^3H_4$ and $^3H_4$ - $^1G_4$, respectively in Tm^{3+} ion. R_1, R_2 and R_3 are the relaxation rate constant of $^3F_4$ - $^3H_6$, $^3H_4$ - $^3H_6$ and $^1G_4$ - $^3H_6$, respectively (includes both nonradiative and radiative). P denotes the excitation power (range from 700 to 18900 W/cm^2), δ is the excitation cross section for Yb^{3+} ion. Then, the steady state population of excited sensitizer ions, N_{Yb}, will be given by:

$$N_{Yb}=\delta P$$

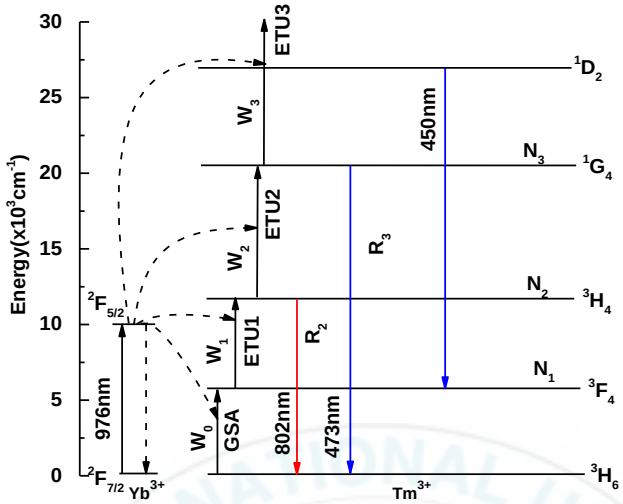

Figure 4.11 Schematic representation of the energy transfer, populating and depopulating processes that can occur in $NaY_{1-x}Yb_xF_4$: Tm^{3+} compound

Following the theory mentioned in ref [13], assume that the population of the state $^3F_4$ (N_1) of the acceptor Tm^{3+} ion scales linearly with the laser power. The steady state N_1 is found that:

$$N_{Yb} \propto N_1$$

Under the assumption described above, the balance equation for the steady state population density of state $^3F_4$, $^3H_4$ and $^1G_4$ can be written as:

$$W_0 N_0 N_{Yb} = (R_1 + W_1 N_{Yb})\, N_1$$

$$W_1 N_1 N_{Yb} = (R_2 + W_2 N_{Yb})\, N_2$$

$$W_2 N_2 N_{Yb} = (R_3 + W_3 N_{Yb})\, N_3$$

From these balance equations, the steady state population density of state N_1, N_2 and N_3 of Tm^{3+} ion are found to be:

$$N_1 = W_0 N_0 N_{Yb} / (R_1 + W_1 N_{Yb});$$

$$N_2 = W_1 N_1 N_{Yb} / (R_2 + W_2 N_{Yb});$$

$$\text{and } N_3 = W_2 N_2 N_{Yb} / (R_3 + W_3 N_{Yb})$$

In the low power density excitation case (less than 4700 W/cm^2) or low Yb3+ concentration doped (5 %), the relaxation from excited states is much stronger than upconversion processes from $^3F_4$ to $^3H_4$ state and from $^3H_4$ to $^1G_4$ state. Thus, upconversion processes can be ignored. In other words, $R_2 >> W_2 N_{Yb}$ and $R_3 >> W_3 N_{Yb}$. Therefore, the steady state population density of state N_2 and N_3 in this case are given by:

$$N_2 = \frac{W_1 N_1 N_{Yb}}{R_2}$$

$$N_3 = \frac{W_2 W_2 N_{Yb}}{R_3}$$

As showed above, $N_1 \propto N_{Yb} \propto P$, thus,

$$N_2 \propto \frac{W_1 N_{Yb} N_{Yb}}{R_2} = \frac{W_1 N_{Yb}^2}{R_2} \propto P^2$$

$$N_3 \propto \frac{W_2 W_1 N_{Yb} N_{Yb}}{R_2} \frac{N_{Yb}}{R_3} = \frac{W_2 W_1 N_{Yb}^3}{R_2 R_3} \propto P^3$$

This implies that in the low power density excitation, an 802 nm emission band requires two energy steps to be excited will have exactly a slope of 2 (for the ideal condition) when the luminescence intensity is plotted in double-logarithmic representation versus absorbed for a pump

power focus. In the theory, the state $^3F_4$ of acceptor Tm^{3+} ion must be at the same energy as the excited state $^2F_{5/2}$ of the sensitizer Yb^{3+} ion, however, in practice, the energy of $^3F_4$ state is smaller than $^2F_{5/2}$ state because of the non-radiative process. Thus the slope values in fact usually are smaller than 2. The slope values for both 653 nm and 473 nm emission bands should be 3 which can be declined to under 3 in the practical measurements.

In the case of high power density excitation (higher than 4700 W/cm^2) or high concentration of Yb^{3+} (20, 50 %), the upconversion processes $^3H_6$ to $^3F_4$ state, $^3F_4$ to $^3H_4$ state and $^3H_4$ to $^1G_4$ state are dominant in comparison with the relaxation processes. It means that $R_2 << W_2N_{Yb}$, $R_3 << W_3N_{Yb}$, the steady state population density of N_2 and N_3 become:

$$N_2 \propto \frac{W_1 N_1}{W_2}$$

$$N_3 \propto \frac{W_2 N_2}{W_3}$$

Because $N_1 \propto N_{Yb} \propto P$ thus:

$$N_2 \propto \frac{W_1 W_{Yb}}{W_2} \propto \frac{W_1 P^1}{W_2}$$

$$N_3 \propto \frac{W_2 W_1 N_{Yb}}{W_3 W_2} \propto \frac{W_1 P^1}{W_3}$$

It can be concluded that in the high power density excitation (higher than 4700 W/cm^2) any emission bands of Tm^{3+} ion (802 nm, 653 nm and 473 nm bands) will have a slope of 1 when the luminescence intensity is plotted in a double-logarithmic representation versus pump power.

5. Conclusion

$NaY_{1-x}Yb_xF_4$: 0.5 % Tm^{3+} crystals with the morphology of hexagonal plates have been synthesized by a facile hydrothermal method. The achieved results of XRD and SEM measurements exposed that the crystal of host matrix and morphology are not impacted by tuning Yb^{3+} ions sensitizer concentration. However, expansion of plates was seen clearly when adjusting the concentration of Yb^{3+} ions.

Under 976 nm excitation pump power, obtained luminescence spectrum and the double logarithmic plots of emission intensities of samples versus pump power are pieces of evidence to verify the effect of high excitation power density, Yb^{3+} ions concentration as well as on luminescent properties of the $NaY_{1-x}Yb_xF_4$: 0.5 % Tm^{3+}. This research may be a material to further understand about the "saturation" phenomenon caused by high excitation power density and sensitizer concentration in the $NaYF_4$: Yb^{3+}/Tm^{3+} compound which has been known as a famous material in biomedical imaging.

References

[1] V.Kale, M. Lastusaari, J. Holsa, T. Soukka, RSC Adv. 5, 35858 (2015).

[2] F. Zhang, Photo Upconversion Nanomaterials (Spring-Verlag, Berlin Heidelberg, 2015).

[3] A. Li, D. Xu, Y. Zhang, Z. Chen, Yuanzhi Shao, J. Am. Ceram. Soc. 99, 1657 (2016).

[4] R.Wang, F.Zhang, J. Mater. Chem. B. 2, 2422 (2013).

[5] M. Nyk, R.Kumar, T. Y. Ohulchansky, E.J. Bergey, P.N. Prasad, Nano Lett. 8, 3834 (2008).

[6] Q.Tian, N.Liu, G.Qin, K.Zheng, D.Zhang, W.Qin, JNN. 11, 6576 (2011).

[7] G. Chen, T. Y. Ohulchanskyy, R. Kumar, H. Agren, Prasas N. Prasad, ACS Nano. 4, 3163 (2010).

[8] L. Liang, H. Wu, H. Hu, M. Wu, Q. Su, J. Alloy. Compd. 59, 2540 (2011).

[9] S. Zeng, F. Ren., C.Xu, J. Alloy. Compd. 59, 2540 (2011).

[10] J. F. Suyver, J. Grimm, M. K. V. Veen, D. Biner, K. W. Kramer, H. U. Gudel, JOL. 117 (2016).

[11] M. Pollnau, D. R. Gamelin, S. R. Luthi and H. U. Gudel, Phys. Rev. B. 61, 3337 (2000).

[12] Y.Lei, H. Song, L. Yang, L. Yu, Z. Liu, J. Chems. Phys. 123 (2015).

[13] J. F. Suyver, A.Aebischer , S.G. Revilla, P. Gerner, H. U. Gudel, Phys. Rev. B. 71 (2015).

[14] Q.Lu, A. H. Li, EPL. 96, 18001 (2011).

[15] K. N. Shinde, S. J. Dhoble, H. C. Swart, K. Park, Phosphate phosphors for solid-state lighting (Springer, 2012).

[16] Cotton. S, Lanthanide and Actinide Chemistry (John Wiley & Son, Ltd,

2006).

[17] H. Guo, N. Dong, M. Yin, W. Zhang, L. Liu, S. Xia, J. Phys. Chems B. 108, 19205 (2004).

[18] F. Wang, X. G. Liu, Chem. Soc. Rev. 38, 976 (2009).

[19] B. S. Cao, Y. Y. He, L. Zhang, B. Dong, JOL. 135, 128 (2013).

[20] D. L. Andrews, G. D. Scholes, G. P. Wiederrecht, Comprehensive Nanoscience and Technology (Elsevier B.V, 2011).

[21] Frank- Michael Matysik, Advances in Chemical Bioanalysis (Springer-
Cham, Heidelberg, NewYork, Dordrecht London, 2014).

[22] L. Prodi, M. Montalti, N. Zaccheroni, Luminescence Applied in Sensor Science (Springer –Verlag, Heidelberg, 2011).

[23] X. Shang, P. Chen, T. Jia, D. Feng, S. Zhang, Z. Sun, J. Qiu, J. Phys. Chems C. 17 (2015).

[24] C. Kittel, Introduction to Solid state physics (John Weley & Son, 2005).

[25] R. D. Shannon, Acta Cryst. A32 (1976).

[26] F. Wang, Y. Han, C. S. Lim, Y. Lu, J. Wang, J. Xu, H. Chen, C. Zhang, M. Hong, X. Liu, Nature. 463, 1061 (2009).

[27] G. Dong, B. Chen, X. Xiao, G. Chai, Q. Liang, M. Peng, J. Qiu, Nanoscale. 4, 4658 (2012).

[28] W. Huang, M. Ding, H. Huang, C. Jiang, Y. Song, Y. Ni, C. Lu, Z. Xu, Mater Res Bull. 48, 300 (2013).

[29] Y. Chen, X. Yan, Q. Liu, X. Wang, J. Alloy. Compd. 562, 99 (2013).

[30] H. Qiu, C. Yang, W. Shao, J. Damasco, X. Wang, H. Agren, P. N. Prasad, G. Chen, Nanomaterials. 4, 55 (2014).

Acknowledgements

I would like to express my deep gratitude to my supervisor, Professor Hyo Jin Seo, who instructed me in during time I did this thesis. He patiently revised the manuscripts over many months without any complaint. This thesis would not have been written without his useful discussions and inspiration from him.

I also would like to extend my sincere thanks to my labmates: Cai Peijing, Lin Qin and Chen Cuily, they helped me very much in doing experiments and analyzing data.

Finally, my great gratitude also goes to those writers whose works I have perused and benefited greatly from without which the completions of thesis would not have been possible.